

## Intra-operative Ischemia Sensing Surgical Instruments

Gregory S. Fischer<sup>1</sup>, Jason Zand<sup>2</sup>, Mark Talamini<sup>2</sup>, Michael Marohn<sup>2</sup>, Takintope Akinbiyi<sup>1</sup>, Kaloyan Kanev<sup>1</sup>, Jennifer Kuo<sup>1</sup>, Peter Kazanzides<sup>1</sup> and Russell Taylor<sup>1</sup>

<sup>1</sup>Johns Hopkins University – CISST ERC, Baltimore-MD, USA

<sup>2</sup>Department of Surgery, Johns Hopkins Hospital, Baltimore-MD, USA

**Abstract** - Surgical techniques rely heavily on adequate visualization of target anatomy. Particularly in laparoscopic and robotic laparoscopic surgery, the operative anatomy and the general view of the operative field is removed from the surgeon's direct vision. Manipulation of peripheral anatomy (i.e. retraction) may lead to ischemia, infarction, and mechanical disruption. The primary goal of our research is to minimize unnecessary damage to manipulated tissue through the incorporation of biofeedback sensors into surgical instruments. We have created "Ischemia Sensing Surgical Instruments" by adapting and incorporating real-time pulse oximetry-like techniques into the working surfaces of operative instruments using custom software and hardware interfaces. The instruments provide real-time tissue oxygenation data directly at the surgical site. In experiments, we monitored porcine hepatic and bowel oxygen saturation during retraction while manipulating the blood supply to the tissue. Results demonstrated a correlation between our measurements and manipulation of the tissue's blood supply.

**Keywords** – Biomedical instrumentation, Ischemia sensing, Pulse oximetry, Surgical instruments, Smart organ retractor.

### I. INTRODUCTION

During surgery, it is common for one organ or structure to visually occlude another in the desired work volume. Therefore, the blocking organ is generally pushed or pulled aside using a retractor. This is common in both the standard open case and the minimally invasive laparoscopic case, though the instruments used are very different. When performing such tissue retraction, however, it is not uncommon to pull too hard or for too long and actually cause damage to the tissue due to lack of oxygen in that area; this is called ischemic tissue damage. There seems to be little literature studying the effects of retraction on

ischemic damage for abdominal surgery, but there is much concern for brain injury such as in [6].

By non-intrusively measuring the oxygen saturation in the tissue being retracted in real-time, it may be possible to help eliminate tissue damage of this type by alerting the surgeon when a dangerous situation arises. In addition to a single measurement directly at the site of retraction, an array of such sensors can be used to give the oxygenation distribution across the retracted surface.

The optimal form of feedback is yet to be determined; it could be in the form of real-time plots of oxygenation trends, video overlay for laparoscopic procedures, or simply visual or audible alerts. Studies of sensory substitution for retraction force come from our group in [1] and [5].

### II. SYSTEM OVERVIEW

Here we present hardware and software development, tool design, and experimental results of a system for measurement of local tissue oxygen saturation levels at the surgical site. Measurement is achieved by affixing oxygenation sensors directly on the distal end of surgical instruments; in particular retractors. This allows for measurement of the oxygenation level of the tissue that is being retracted without intruding on the standard workflow of a surgical procedure.

The procedure used for determining tissue oxygen saturation is similar to that of pulse oximetry, with the exception that there is not necessarily a pulse that the algorithm can be based on. Therefore, rather than detecting a pulse and taking the differences between the received signals during systole and diastole which gives the arterial oxygen saturation level ( $S_aO_2$ ), the results are purely based on the attenuation of light through the tissue. The other deviation from standard pulse oximetry is that we do not



Fig. 1. Ischemia sensing laparoscopic Babcock grasper

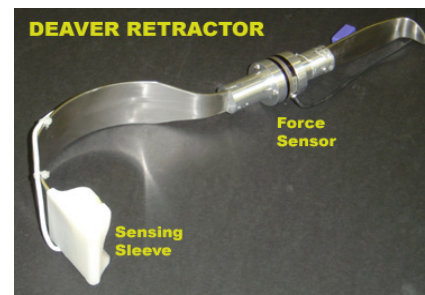


Fig. 2. Instrumented ischemia and force sensing Deaver retractor.

usually have the luxury of placing the emitter and the receiver in an opposing configuration; therefore, the light must be capable of diffusing through the tissue and being picked up by a receiver that is positioned laterally to it. A slight angle towards each other is beneficial, but anything too significant could alter the functionality of the tool, and in fact could cause more ischemic damage. Therefore, we have to deal with much greater susceptibility to noise due to a much lower signal-to-noise ratio (SNR). In a prototype retractor (See Fig. 2), we built a plastic sleeve with a slightly curved face to give the emitter and receiver a slight angle towards each other. The sleeve slips over the distal end of a Deaver retractor, with the sensors embedded flush with the working surface.

This technology has potential widespread use for a large variety of surgical procedures. The primary focus of this work is for aiding in abdominal surgery, in particular working with the liver and bowels. Fig. 1 displays one of two prototype, instrumented retractors. This one is a laparoscopic Babcock retractor whose primary purpose is retraction of the bowels during minimally invasive surgery (MIS) procedures. The second retractor, shown in Fig. 2, is a Deaver retractor; it is a modified version of the standard tool for retraction of the liver during open surgery. This tool has been fitted with a plastic sleeve that incorporates the ischemia sensors. The device also contains a 6 DoF ATI force/torque (FT) sensor, which can be used for studying the relationship between ischemia and retraction force. In addition, this fixture would be ideal for aiding in training procedures.

### III. DEVICE FUNCTIONALITY

The goal of the device is to determine the oxygen saturation ( $SO_2$ ) of the blood in the tissue of interest. In order to sense the  $SO_2$ , we take advantage of the light absorption properties of the tissue. Attenuations of different wavelengths of light are a function of the relative concentrations of deoxygenated hemoglobin (Hb) and oxygenated hemoglobin ( $HbO_2$ ) in the blood. By picking two or more wavelengths of light, we monitor their

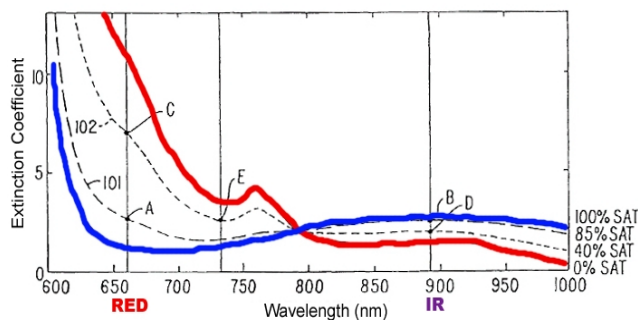


Fig. 3. Relationship between light attenuation and light wavelength as oxygen saturation is varied (Original plot courtesy of Nellcor [3]).

respective attenuations relative to each other can be monitored and used to get a value proportional to the oxygen saturation. This is the same principle upon which pulse oximetry is based, but we have made necessary application-specific modifications to the standard procedure. Fig. 3 shows a plot of the attenuation of light passing through tissue as a function of wavelength. By comparing the trends for different values of the relative concentrations of Hb and  $HbO_2$  in the blood, it is clear that if we monitor the attenuation of one wavelength from each side of the 'crossover point' at the isobestic (equiconcentration) wavelength ( $\sim 805nm$ ), it should be possible to resolve the relative oxygenation level.

The emitters are bi-polar / bi-color LEDs that produce red ( $\lambda_{Red} = 660nm$  peak) and infrared ( $\lambda_{IR} = 895nm$  peak) light. By using these wavelengths, it is clear from Fig. 3 that if the oxygen saturation drops, the attenuation of red light should increase and that of IR light should decrease. It is precisely this change that provides the information necessary to calculate  $SO_2$ . Experimental measurements that confirm this response are shown in Fig. 4. The photodiode response corresponding to LED transmission through the tissue at  $\lambda_{IR}$  and  $\lambda_{Red}$  is measured on a finger when blood supply is cut off. The values on the plot represent the normalized photodiode responses,  $\tau_{Red}$  and  $\tau_{IR}$ , where supply was cut off at 20 seconds and restored at 90 seconds as shown with a 2 second moving average filter.

The reason for using a bi-color LED as the emitter is two-fold: 1) LEDs are very compact, low cost, and provide for the possibility of disposable sensors, and 2) they allow for the red and IR light to come from the same physical location, thus allowing the light from both wavelengths to traverse the same path through the tissue. Other solutions involving lasers, fiber optics, or narrow-band optical filters may prove to be useful, but add significant complexity to the system. Measurements are obtained using silicon photodiodes tuned for the appropriate range of wavelengths. Again, other detection solutions exist, but photodiodes provide for low cost, compact, accurate measurements.

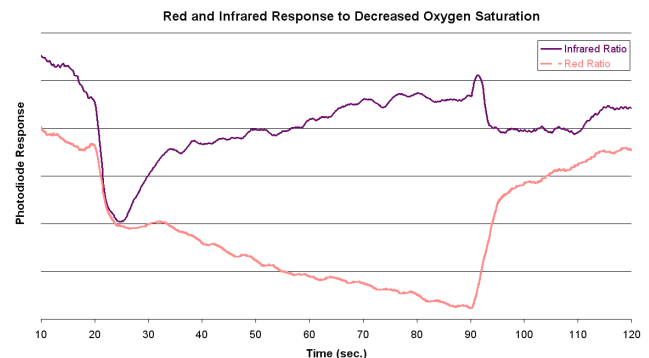


Fig. 4. Experimental validation of Red and IR responses ( $\tau_{IR}$  and  $\tau_{Red}$ ) as blood supply is cut off and restored.

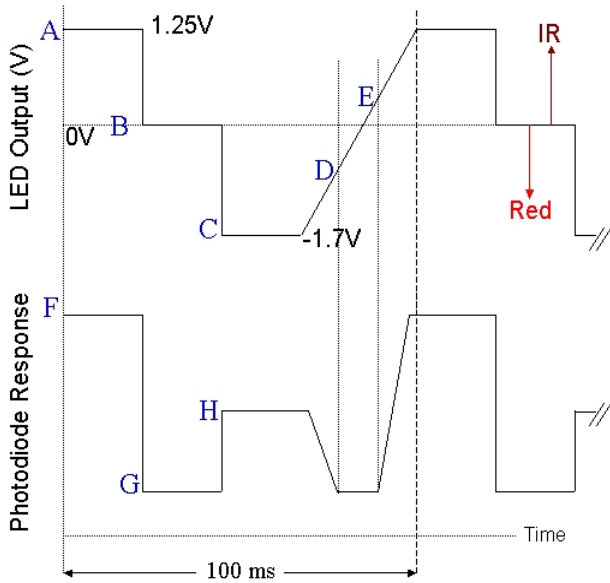


Fig. 5. System LED output and typical photodiode input description.

In order to determine the tissue oxygen saturation level, we use the following algorithm:

- 1) Output IR light (*A*) and monitor the response (*F*)
- 2) Turn off output (*B*) and monitor the response (*G*)
- 3) Output Red light (*C*) and monitor the response (*H*)
- 4) Ramp light intensity from full Red (*C*) to Off (*B*)
  - Determine where the response is lost (*D*)
- 5) Ramp light intensity from Off (*B*) to full IR (*A*)
  - Determine where the response is regained (*E*)

Fig. 5 shows the LED output and the corresponding simulated photodiode response. The letters represent the values used in the following equations. The letters *A* thru *E* represent output voltages proportional to the drive current for the LEDs. The letters *F* thru *H* represent the photodiode response; since all inputs come from the same photodiode and pass through the same amplifier, the units are irrelevant. The ratios of the input signal to the emitted light are calculated for both  $\lambda_{IR}$  and  $\lambda_{Red}$ . These ratios,  $\tau$ , are the inverses of the light transmission,  $T$ , where  $P_0$  represents the incident light intensity and  $P_t$  represents the transmitted light intensity. The equations in terms of the above plots are shown in (1) and (2) respectively.

$$\tau_{IR} = (T_{IR})^{-1} = \frac{F - G}{A - E} = \frac{P_0(\lambda_{IR})}{P_t(\lambda_{IR})} \quad (1)$$

$$\tau_{Red} = (T_{Red})^{-1} = \frac{H - G}{|C - D|} = \frac{P_0(\lambda_{Red})}{P_t(\lambda_{Red})} \quad (2)$$

We define the “Relative Oxygen Saturation,”  $R$ , as the ratio of  $\tau_{Red}$  to  $\tau_{IR}$ .

$$R = \frac{\tau_{Red}}{\tau_{IR}} \quad (3)$$

This allows us to see trends in the tissue oxygenation level with relatively simple computations that can easily be performed rapidly on an embedded microprocessor. Since we are primarily concerned with trends, this definition is usually sufficient. Note that there are constants that must be inserted into (1) and (2); they are to account for non-uniformities in the spectral response of the photodiode and for the differences in LED intensities for  $\lambda_{IR}$  and  $\lambda_{Red}$ . They have been left out of the equations for simplicity, but can be easily determined from the component datasheets.

In order to determine the true oxygen saturation, we must determine the relationship between the red and infrared light transmission and  $SO_2$ . In general, we have (4); now we must determine what model to use.

$$SO_2 = f(\tau_{Red}, \tau_{IR}) \quad (4)$$

According to [2], and similarly in [4] and [7], the mapping from the ratio of optical densities ( $OD$ ) to  $SO_2$  is as follows in (5).  $A$  and  $B$  are coefficients that must be obtained through calibration, and  $OD$  represents the optical density as shown.

$$SO_2 = A - B \left( \frac{OD(\lambda_{Red})}{OD(\lambda_{IR})} \right) = A - B \left( \frac{\log(R_{Red})}{\log(R_{IR})} \right) \quad (5)$$

This model is linear in the ratio of optical densities, and the values for  $A$  and  $B$  can be found using simple linear regression techniques. This calibration can be made when measurements of our system are collected along with a synchronized baseline measure from another calibrated device.

#### IV. HARDWARE INTERFACE

Early prototypes of the device utilized PC-based off-the-shelf data acquisition (DAQ) hardware with simple additional stand-alone circuitry. Due to issues of reliability, cost, noise, lack of modularity, and lack of application-specific hardware, we opted to design a custom hardware interface.

Shown in Fig. 7 is a photograph of the “Smart Retractor Interface” (SRI) circuit board. The system is essentially a programmable DAQ system specifically designed for our needs. The SRI unit is interfaced to the PC via USB; this allows for many such boards to be used simultaneously, each with its own address using a standard USB hub.

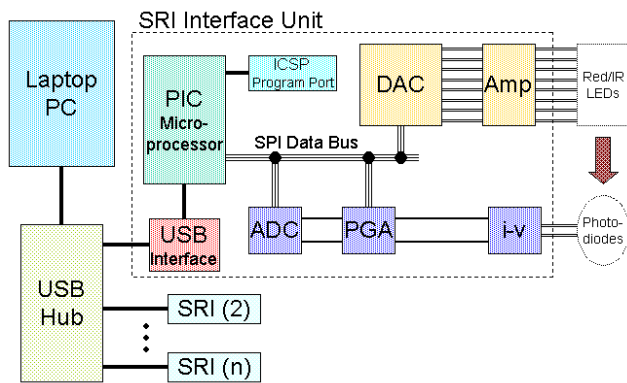


Fig. 6. Hardware block diagram.

The design layout of the system is shown in the block diagram in Fig. 6. The heart of the system is a Microchip PIC processor, which is configured such that it can be programmed via ‘In Circuit Serial Programming’ (ICSP); this allows for easy modification of the code, even when performing tests in the OR. Communication to an external PC, including input commands and data transfer, is through a USB interface. The choice to use USB is twofold: 1) it allows the use of many interfaces simultaneously on a standard, OS independent laptop PC, and 2) 5V power can be obtained directly from the PC with no additional cabling.

The SRI supports up to eight differential analog outputs to drive combined bi-polar LED’s (or 16 single-ended outputs for more general purposes). The Digital to Analog converter (DAC) outputs drive the red and infrared LEDs with up to 100mA (after amplification) with 14-bit precision (0-5V range). The interface also supports two analog inputs for the photodiodes. This allows for retractors with several sets of LEDs and photoreceptors on their working surface that can provide the distribution of oxygen saturation across the tissue.

The receiver silicon photodiodes are operated in a photovoltaic, zero-bias mode. The current received is measured after being converted to a voltage via a transimpedance amplifier circuit (i-v). In order to account for variable reception levels due to different types and thicknesses of tissues this signal is passed through a programmable gain amplifier (PGA). This allows us to utilize the full analog input range (0-4.096V) and increase the signal-to-noise ratio (SNR). The signal is digitized via one of the two 16-bit analog inputs on the Analog to Digital converter (ADC). Communication between the PIC microprocessor and the DAC, ADC, and PGA is via the SPI serial communication bus with the appropriate chip-select lines (not shown in Fig. 6).

With a simple configuration change on the board, the SRI can also be used as a standard DAQ unit. In this mode there are 16 analog outputs with 14-bit precision (0-5V), and two high-resolution, 16-bit analog inputs. The inputs are

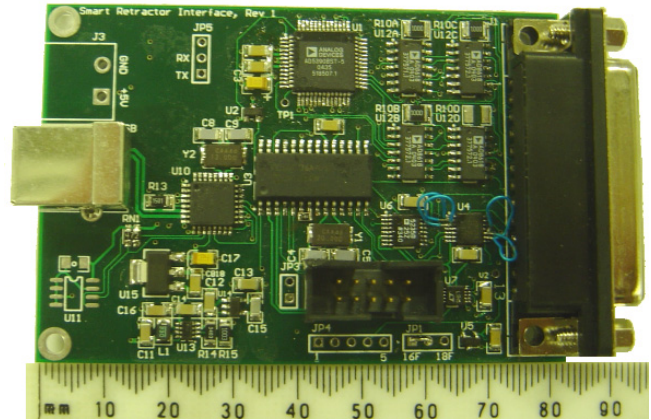


Fig. 7. Custom USB hardware interface for ‘Smart Organ Retractor’.

still amplified via a programmable gain amplifier, and therefore can be scaled to use this full range. An important application for this is for measuring retraction force data obtained through strain gages and load cells.

## V. RESULTS

The initial application for the system is for monitoring and preventing ischemic damage due to retraction during abdominal surgery. A primary goal is to monitor oxygen saturation in liver tissue. Therefore, the bulk of the experiments to date are concerned with liver in an *in vivo* porcine model. In one set of experiments, we take a Deaver retractor (a standard for open abdominal surgery) and fit it with a sensing sleeve that incorporates a bi-polar LED and a photodiode (Fig. 2) embedded into the surface. This plastic sensing sleeve represents a disposable sleeve that could be placed on a wide array of standard surgical retractors.

In the experimental protocol, the retractor is placed on the surface of the liver as shown to the left in Fig. 8. It is held manually, and we let it sit until the signal settles. The blood supply to the liver is then occluded by applying the Pringle maneuver. This maneuver allows the surgeon to stop the arterial inflow to the liver by manually squeezing the porta hepatic without causing permanent damage to the vessel. The relative oxygen saturation level is monitored in real-time and displayed for the surgeon as shown in Fig. 10. Also, all raw data is logged throughout the experiment for later analysis. After a set time, blood flow is restored to the tissue by releasing the vessel, and oxygen saturation is monitored as  $O_2$  returns to the tissue as it becomes reperfused.

The plot shown on the right of Fig. 8 displays results from one trial where the instrumented Deaver retractor is used to retract a portion of liver, and while the tissue is being retracted a surgeon periodically cuts off and restores the liver’s arterial supply as mentioned above. The vertical lines on the plot represent the locations where the blood supply was cut off (dashed, red) and restored (solid, blue).

While still focusing on abdominal procedures, further experiments were performed to validate the possibility of instrumenting laparoscopic instruments with ischemia sensors. The first prototype device to act as a proof-of-concept for laparoscopic MIS procedures was targeted at bowel retraction. This first device was based off a standard Ethicon laparoscopic Babcock retractor that has been instrumented with oxygenation sensors as discussed previously. The device is shown in Fig. 1. This device not only provides for a first trial of a laparoscopic instrument, but also provides for a representative trial of grasping laparoscopic tools.

As before, we performed experiments with this retractor where the blood supply was periodically cut off and restored as the oxygen saturation was monitored. The results using this retractor are presented in Fig. 9. For these trials, a section of bowel was isolated completely from the rest of the bowel such that the only blood supply source to the tissue was from the associated section of the mesentery. Since the tissue is isolated, by manually occluding the arterial supply through the mesentery, the tissue becomes deoxygenated and hypoperfused. This allowed for a very

controlled experiment.

The results look very promising; in fact, these results seem even better than those for the liver. This is most likely due to the much more controlled nature of the experiment. As before, the blood supply was periodically cut off and restored while the retractor/grasper was attached to the tissue. Again, the vertical lines on the plot represent the locations where the blood supply was cut off (dashed, red) and restored (solid, blue).

Both this plot and the previously mentioned results are passed through a five second moving average filter to smooth the results; this is appropriate since we do not expect immediate changes in  $SO_2$ . In fact, the later results were quite good even without a smoothing filter. This is most likely because of the significantly higher SNR obtained when measuring though the much less optically dense bowel than in the very solid, dark liver tissue. This is an important result that indicates that it is very important to have LEDs that have sufficient brightness to penetrate the tissue; when this is not the case, ambient light (especially bright OR lights) can dominate the signal, causing poor results.

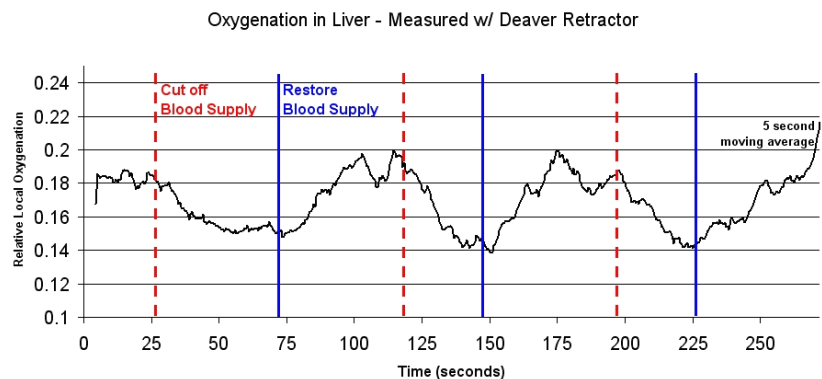
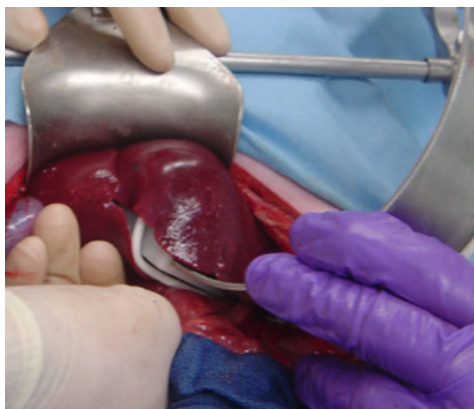


Fig. 8. Representative oxygen saturation results of liver retraction with instrumented Deaver retractor while manipulating tissue blood supply.

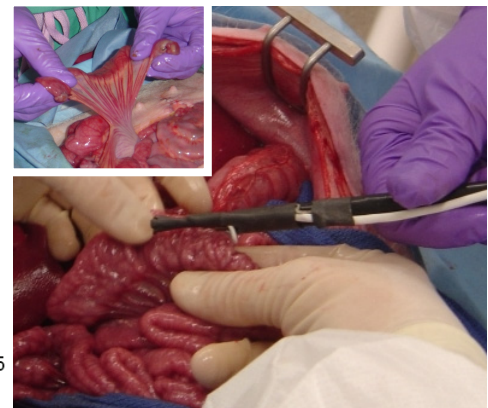
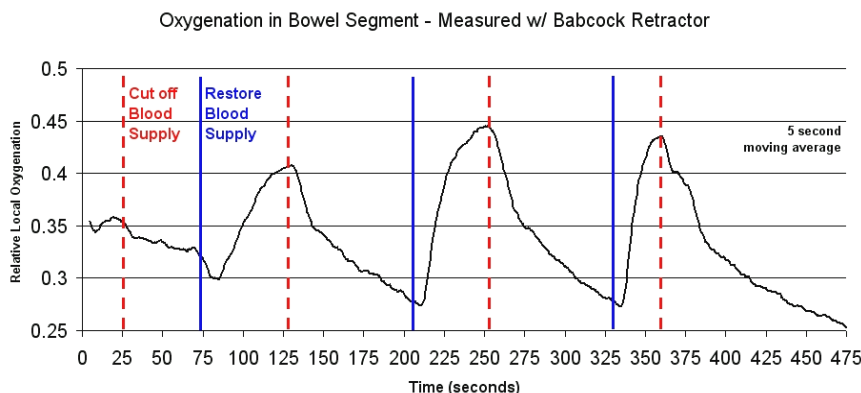


Fig.9. Oxygen saturation in an isolated bowel segment (see inlay) measured with instrumented Babcock retractor while manipulating blood supply.



Fig. 10. Overview of 'Smart Retractor' in use in the OR.

## VI. DISCUSSION

We have developed a system for measuring relative oxygen saturation of internal tissue intra-operatively. The system comprises of instrumented standard surgical tools, a custom, programmable hardware interface, and PC-side control and visualization software. The system had been tested under several retraction scenarios including liver and bowel manipulation. We have developed prototype instruments designed for both open and MIS laparoscopic procedures. Fig. 10 shows the system in use in the OR during *in vivo* porcine experiment in the Johns Hopkins Minimally Invasive Surgery Training Center (MISTIC) center. Results thus far seem quite promising in that as oxygenation levels of tissue are intentionally decreased and restored, the system can track and visualize the information as shown in Fig. 8 and Fig. 9.

Such a system will be very useful during surgery because it can monitor local tissue oxygen saturation and warn the surgical staff of any damage as it begins to occur. Further, it performs this task with minimal intrusion into the standard operating procedure and involves the use of cheap, possibly disposable, additions to standard surgical instruments. More complex designs in the process of being tested incorporate a grid of such sensors on the working surface of the retractor and allow measurements of a distribution of  $O_2$  saturation across the tissue (as opposed to a single point).

This system, in addition to being used during surgical procedures as a method for warning the surgeon about dangerous levels of ischemia, may prove as an invaluable

aid for teaching OR staff and residents proper retraction techniques. By measuring the trends in oxygen saturation and the forces used during retraction, great insight could be gained by having quantitative feedback on retraction outcomes.

Further, there is very little literature studying standard forces applied during retraction. This system, with the incorporated force sensing capabilities, will allow clinicians to determine the effects of time and force of retraction on local tissue oxygen saturation and ischemic damage. Using this information, feedback for novice and experienced surgeons alike can be obtained. Performing these trials and determining the correlations between oxygen saturation and time and force of retraction is in the next phase of this project.

## ACKNOWLEDGMENT

The authors would very much like to acknowledge the assistance of the Johns Hopkins Minimally Invasive Surgery Training Center (MISTIC) and doctors Samuel Shih, Alexander Aurora, Joseph Fuentes, and Eric Hanly for assistance and guidance with the experiments in the OR. We would also like to thank Hamid Wasti for assistance with design of the hardware interface, and Byte Craft Limited (Waterloo, Canada) for donating the PIC compiler software. Partial funding for this project was provided by NSF Engineering Research Center Grant #EEC-97-31478 and Johns Hopkins Internal Funds.

## REFERENCES

- [1] T. Akinbiyi, A.M. Okamura, and D.D. Yuh, *Dynamic Augmented Reality for Haptic Display in Robot-Assisted Surgical Systems*, Medicine Meets Virtual Reality 13, J. D. Westwood, et al. (Eds.), IOS Press, 2005.
- [2] J. Enderle, S. Blanchard, and J. Brozino, *Introduction to Biomedical Engineering*, San Diego, CA: Academic Press, 2000.
- [3] J. Casciani, P. Mannheimer, S. Nierlich, and S. Ruskewicz, *Pulse Oximeter and Sensor Optimized for Low Saturation*, US Patent 6,272,363 B1, August 2001.
- [4] P. Mannheimer, J. Casciani, M. Fein, and S. Nierlich, *Wavelength Selection for Low-Saturation Pulse Oximetry*, IEEE Transactions on Biomedical Engineering, vol. 44, no. 3, pp. 148-158, March 1997.
- [5] S. Prasad, M. Kitagawa, G. Fischer, J. Zand, M. Talamini, R. Taylor, and A. Okamura, *A Modular 2-DOF Force-Sensing Instrument For Laparoscopic Surgery*, Sixth International Conference on Medical Image Computing and Computer-Assisted Intervention, vol. 2878, pp. 279-286, November 2003.
- [6] J. Zhong, M. Dujovny, A. Perlin, E. Perez-Arjona, H. Park, and F. Diaz, *Brain Retraction Injury*, Neurological Research, vol. 25, no. 8, pp. 831-838, December 2003.
- [7] G. Zonios, U. Shankar, and V.K. Iyer, *Pulse oximetry theory and calibration for low saturations*, IEEE Transactions on Biomedical Engineering, vol. 51, no. 5, pp. 818-822, May 2004.